

Thermal Stresses Associated with Part Overhang Geometry in Electron Beam Additive Manufacturing: Process Parameter Effects

Bo Cheng and Kevin Chou

Mechanical Engineering Department
The University of Alabama
Tuscaloosa, AL 35487

REVIEWED

Abstract

For powder-bed electron beam additive manufacturing (EBAM), support structures are required when fabricating an overhang to prevent defects such as curling, which is due to the complex thermomechanical process in EBAM. In this study, finite element modeling is developed to simulate the thermomechanical process in EBAM in building overhang part. Thermomechanical characteristics such as thermal gradients and thermal stresses around the overhang build are evaluated and analyzed. The model is applied to evaluate process parameter effects on the severity of thermal stresses. The major results are summarized as follows. For a uniform set of process parameters, the overhang areas have a higher maximum temperature, a higher tensile stress, and a larger distortion than the areas above a solid substrate. A higher energy density input, e.g., a lower beam speed or a higher beam current may cause more severe curling at the overhang area.

Keywords: Electron beam additive manufacturing, Overhang, Thermomechanical simulation

1. Introduction

The powder-bed electron beam additive manufacturing (EBAM) technology utilizes a high-energy source to fabricate metallic parts, layer-wise, by sintering and/or melting metal powder. EBAM offers a unique combination of process flexibility, time savings, and reduced costs in the production of complex-shaped small-batch metallic components. EBAM has several advantages. First, EBAM is one of a few AM technologies capable of making full-density functional metallic parts. Second, build part properties are comparable or even better than parts made by conventional means. In addition, the process is carried out in vacuum at an elevated temperature allowing parts free from impurity and with reduced residual stresses. EBAM has been increasingly used in aerospace and medical fields [1-3]. Since EBAM can reach very high temperatures, a variety of metal-based materials have been studied including Ti-6Al-4V, tool steels [4], copper [5], and nickel-based super alloys [6], etc.

Despite extensive advantages over conventional technologies, EBAM still encounters several process and part deficiencies such as layer delaminations and distortions [7]. Hence, accurate physical models of both heat transfer and mechanics analyses are required to investigate the thermomechanical phenomena in EBAM and to correlate process parameters with the occurrence of the deficiencies. Although there has been an increasing interest in the study of the EBAM process, the primary focus has been different materials and applications, build part

microstructure and properties, while process physics modeling of the EBAM process has been few. There were recently some finite element (FE) modeling work about the EBAM process such as Zäh and Lutzmann [7], Mahale [8], Jamshidinia et al. [9], Shen and Chou [10], and Cheng and Chou [11], However, mainly focused on the thermal aspect of the EBAM process.

The laser-based metal additive manufacturing studies is first reviewed below since there are relatively more studies of experimental and finite element (FE) modeling work in this field. In a multi-layer laser Direct Metal Deposition (DMD) process, Liu et al. [12] presented a 3D sequentially coupled thermo-mechanical FE model to predict residual stresses and deformations. Temperatures, residual stresses and part deflections were investigated. Based on the simulation results, the cooling rate in DMD can be as high as 3000 K/s. Kamara et al. [13] investigated the residual stresses generated from the deposition of multiple-layer wall of a Waspaloy structure on an Inconel 718 substrate in a laser DMD process. The residual stress characteristic in the wall (20 layers, each with 6 parallel tracks) was studied using ANSYS. The simulation results revealed that the stress along the length of the wall oscillated about a stress-free state while the stress was found to vary with positions along the height of the wall. The tensile stress in scanning direction of the deposited wall increased with the number of layers; on the contrary, the stress in the building direction of the wall was close to zero. Of a Wire and Arc Additive Layer Manufacturing (WAALM) study, Ding et al. [14] utilized an FE method to study the thermomechanical responses of large multi-layer wall shaped WAALM structures. The simulation results of temperature distributions, stress distributions and distortions were verified by experiments. The stress across the deposit was uniform with very little influence of succeeding layers. In addition, Clamping or unclamping significantly affected the stress redistribution. In a study of Selective Laser Melting (SLM), Zaeh and Branner [15] investigated the effect of the layer thickness on T-shaped cantilever part deformations using a 3D FE thermomechanical model. The simulations indicated that a smaller layer thickness was responsible to larger deformations due to that the input energy had to be distributed into reduced layer volumes. Dai and Shaw [16] numerically investigated the effect of laser scanning strategy on residual thermal stresses and distortions of a flat nickel plate in ANSYS. The findings revealed that proper laser scanning patterns could result in less out-of-plane distortions. Nickel et al. [17] presented a 3D FE study on the deposition pattern of laser deposited metal parts produced by the shape deposition manufacturing (SDM). The results clearly pointed out that the deposition pattern had a significant effect on part deflections. Specifically, for a plate geometry, a raster pattern with lines oriented 90 degree from the beam's long axis produced the lowest deflections for a beam substrate, while the spiral pattern scanned from the outside to the inside produced low and uniform deflections. Matsumoto et al. [18] proposed an FE method for calculating the distribution of temperatures and stresses within a single metallic layer formed on the powder bed in SLM. The study showed that the stress distribution in the solidified part caused by temperature changes during forming showed a stripe pattern of compressive and tensile stresses. The deflection of the solid layer increased as the track length increased. In addition, when the neighboring track began to solidify, a large tensile stress between the solidified tracks appeared at the side end of the solid part.

On the other hand, only limited literature in the study of thermomechanical process of EBAM was found. Shen and Chou [19] developed a coupled thermomechanical finite element model to simulate the transient heat transfer, part distortion and residual stresses of crossed raster

scanning during the EBAM processing of Ti-6Al-4V powder. The coupled mechanical simulation captured the evolution of the residual stresses and part distortions during different process stages such as preheating and melting scans. For an overhang structure, based on the developed model [19], Cheng et al. [20] further improved the model to simulate the thermomechanical phenomenon of a multi-scan 2 layers depositions of an overhang in the EBAM process. The results showed that the poor thermal conductivity of Ti-6Al-4V powder leads to higher temperatures in the overhang areas and in the associated higher residual stresses after final cooling. In addition, a smaller porosity (e.g., 35% vs. 50%) could reduce the process temperatures as well as residual stresses in the build part.

Since an overhang (or down-facing) geometry is a common feature in many engineering components and fabricating an overhang part can be challenging, this study attempted to investigate the thermomechanical phenomenon associated with building an overhang part in EBAM. Figure 1 show (a) a CAD model of a part with overhang features and (b) an image of the EBAM fabricated part, showing noticeable distortions in the overhang area [20]. Due to the nature in building an overhang, one portion of the part was deposited upon a powder substrate, while another portion was deposited on a previously solidified substrate. Consequently, different thermal properties between the solid and powder materials resulted in different thermal responses, and then different stress and distortion conditions. An FE model was developed to simulate the thermal and mechanical responses in fabricating overhang layers in EBAM. The objectives were to evaluate temperature and stress distributions as well as distortions associated with an overhang build and to study process parameter effects on the severity of residual stresses and overhang distortions such as curling.

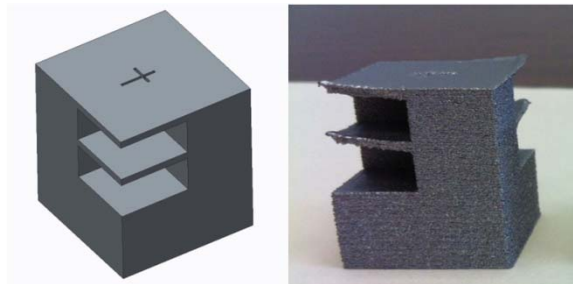


Figure 1. Distortions in an overhang area of an EBAM built part [20].

2. Finite Element Modeling for Overhang Study

2.1 Model Configuration

A 2D finite element thermomechanical model was developed using ABAQUS to simulate the temperature, residual stress distributions and deformations of an overhang part model. Figure 2 shows the geometric details of the overhang model; it has a substrate dimension of 17.6 mm × 10 mm (Length×Height) excluding the surrounding powder bed. The substrate was composed of half powder and half solid, and the powder layers were composed of Ti-6Al-4V particles with 50% porosity. A thin layer, on the top of the substrate, is assumed to be the latest added powder layer. A conical body heat source with linearly decaying along the depth direction (Y); scanning along the X direction was applied on the top powder layer.

The major analysis steps consisted of a preheating cycle, an electron beam scanning cycle and a cooling cycle. The preheating cycle is simplified as the thermal initial conditions for both the substrate and the powder layer, assigned with a uniform temperature distribution of $T_{preheat}$. The electron beam moving and heating will be initiated at the scanning cycle. Due to vacuum, convection between the powder layer and surroundings is ignored; only radiation is considered in heat transfer between the part and environment. The temperature of the substrate bottom is confined as a constant temperature of $T_{preheat}$ as the thermal boundary condition. The electron beam scanning occurs at the top surface of a powder layer and traverses along the X-axis with a constant speed. All the mechanical degrees of freedom are confined at the bottom of the solid substrate. In order to save computational time and keep good model accuracy, a finer mesh was applied in the beam scanning path to directly incorporate the incident Gaussian beam heat flux region while a coarser mesh was used in regions away from high beam energy affected zone. The mesh size of the scanning path is $0.2 \text{ mm} \times 0.07 \text{ mm}$ (X×Y).

During the cooling cycle, all the materials were assumed to be simply under the cooling process until the temperature drops to the room temperature of $20 \text{ }^\circ\text{C}$. The displacement constraints at the solid substrate bottom are kept. The thermal boundary condition was pure radiation on the top surface. Detailed modeling parameters are listed in Table 1 below.

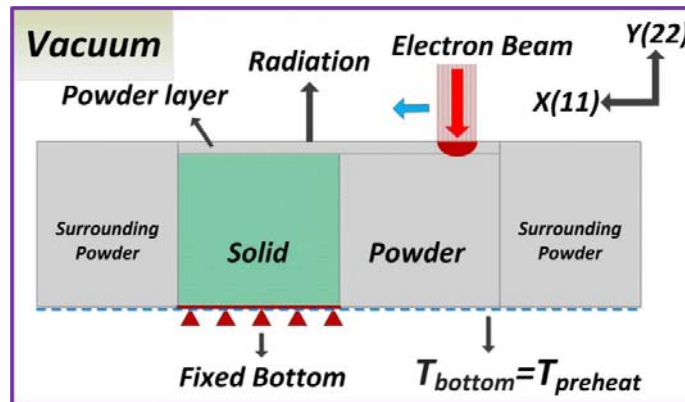


Figure 2. Model configuration and BCs in electron beam scanning cycle.

Table 1. Parameters Used in Simulations.

Parameters	Values
Solidus temperature, T_S ($^\circ\text{C}$)	1605 [21]
Liquidus temperature, T_L ($^\circ\text{C}$)	1655 [21]
Latent heat of fusion, L_f (kJ/Kg)	440 [21]
Electron beam diameter, Φ (mm)	-
Absorption efficiency, η	0.9 [22]
Scan speed, v (mm/sec)	-
Acceleration voltage, U (kV)	60 [23]
Beam current, I_b (mA)	-
Powder layer thickness, t_{layer} (mm)	0.07
Porosity, ϕ	0.5
Beam penetration depth, d_p (mm)	0.062[7]
Preheat temperature, $T_{preheat}$ ($^\circ\text{C}$)	750

2.2 Model Examination

Due to lack of literatures on EBAM thermomechanical studies, a 3D welding thermal mechanical simulation study of Inconel 718 [24] has been used to validate the model. Deshpande et al. [24] developed a thermomechanical analysis model using ABAQUS and SYSWELD to study the temperature and stress distributions in a welding process using Inconel 718. The same modeling method used in the aforementioned 2D EBAM overhang model was utilized to duplicate a 3D welding coupled thermomechanical model. The simulation results have been analyzed and compared with results from Deshpande et al. [24]. Figure shows the butt welding geometry, temperature analysis point and stress analysis location. Figure Figure 4 compares the simulated thermal history of Node C on the plate top surface as shown in Figure 3. Figure 5 compares simulated residual stresses without non-linear geometry effect from the authors and from Deshpande et al. [24]: (a) transverse stress along the weld line, (b) longitudinal stress along the weld line, (c) transverse stress along the transverse direction, and (d) longitudinal stress along the transverse direction. The thermal and residual analysis results of the duplicated model are fairly close to the literature values. Therefore, the thermomechanical FE model developed was used to conduct the thermomechanical analysis of EBAM.

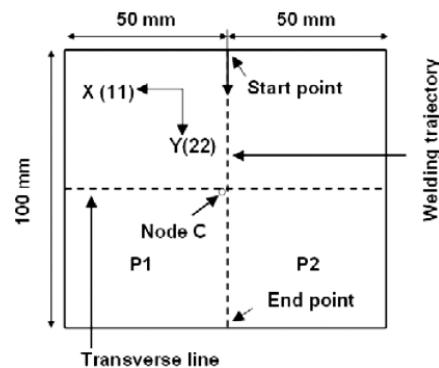


Figure 3. Schematic representation of a butt joint welding (two piece, P1 and P2) from Deshpande et al. [24].

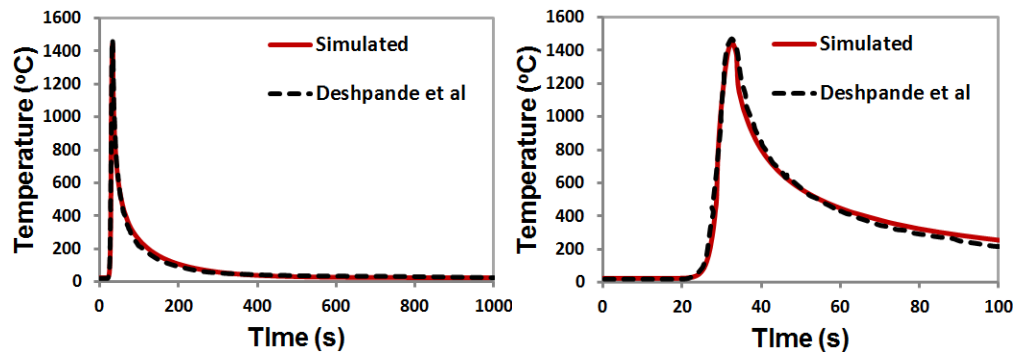


Figure 4. Simulated thermal analysis results compared with Deshpande et al. [24].

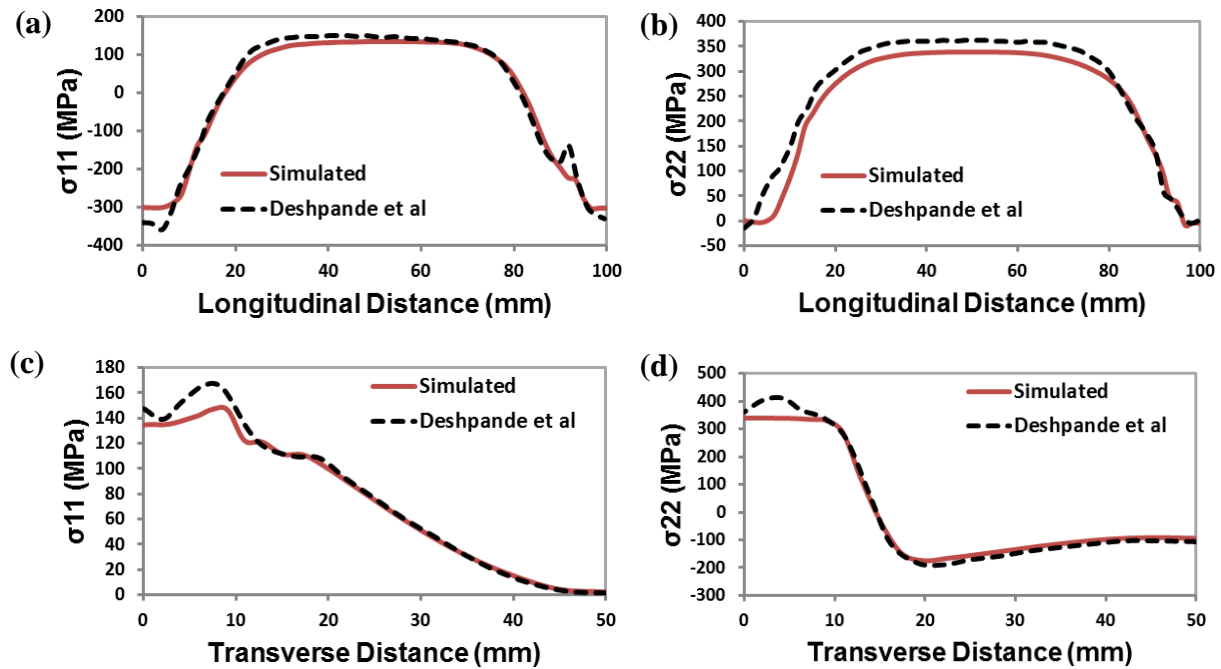


Figure 5. Simulated stress analysis results compared with Deshpande et al. [24].

3. Design of Experiments Study

The energy density (E) may be an efficient way for the measurement of averaged applied energy per unit volume of materials during the beam scanning process. Equation (1) below was used to describe the energy density in the beam melting process [25,26]:

$$E = \frac{P}{v \cdot h \cdot t}, \quad (1)$$

where P is the beam power (J/s), v is the scanning speed (m/s), h is the hatch spacing (m) and t is the layer thickness (m). It is noted that energy density is proportional to the beam power, while the beam scanning speed, the hatch spacing as well as the powder layer thickness have an inverse relationship with the energy density. Since this study is focused on a 2D approach, the hatch spacing effect is not considered. On the other hand, the beam diameter is included for the energy density consideration, Therefore, Eqn (1) for EBAM can be written as:

$$E = \frac{U \cdot I}{v \cdot D \cdot t}, \quad (2)$$

where U is electron beam voltage (V), I is beam current (A) and D is beam diameter (m), others are the same as aforementioned. Thus, based on the energy density Eqn (2), it is possible to conduct a numerical study of factorial experiments on the process parameters effects on the temperature, thermal stress and deformations. Three process parameters were considered as the factors; they are the beam scanning speed (V), the beam diameter (D) and the beam current (I). Two levels (high and low), covering a reasonable range, were designated for each parameter. The ranges of the parameters are listed in Table 2. A full factorial experiment, i.e., total 8 sets of simulations, was conducted. The spread sheet of the factor selection is shown in Table 3.

Table 2. Range of Values for Each Process Parameters Studied.

<i>Process parameters</i>	<i>Low Level (-)</i>	<i>High Level (+)</i>
Speed (mm/s)	400	1000
Diameter (mm)	0.4	0.8
Current (mA)	6	10

Table 3. Factor Selections of Each Experiment Case.

Case No.	<i>V</i>	<i>D</i>	<i>I</i>	<i>V</i>	<i>D</i>	<i>I</i>
1	-	-	-	400	0.4	6
2	+	-	-	1000	0.4	6
3	-	+	-	400	0.8	6
4	+	+	-	1000	0.8	6
5	-	-	+	400	0.4	10
6	+	-	+	1000	0.4	10
7	-	+	+	400	0.8	10
8	+	+	+	1000	0.8	10

4. Results and Discussion

4.1 Thermal stress formation mechanism

The thermally induced stresses can be explained from temperature gradients [27]. Due to the rapid heating of the upper surface by the fast moving electron beam and the relatively slow heat conduction, a steep temperature gradient develops. Then the expansion of the heated top layer is restricted by the underlying material, which has a lower temperature, and counter compressive strains are induced. Therefore, without mechanical constraints on the top surface a counter bending away from the electron beam can be expected. In the cooling period, the compressed upper layers start shrinking and a bending angle towards the beam develops due to no bonding on the scan end location. Figure 6 shows the temperature gradient induced deformation.

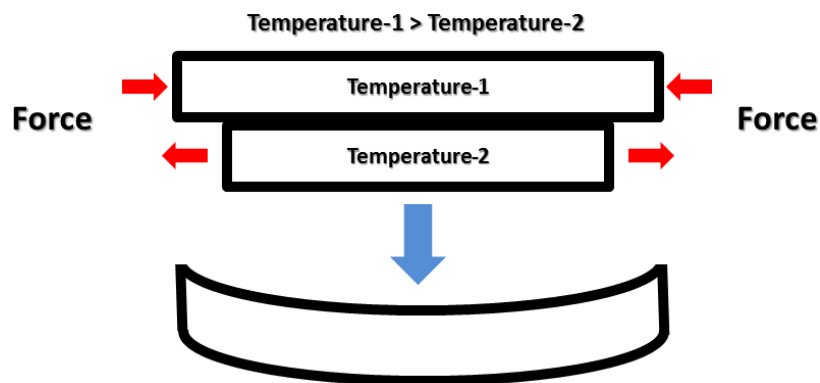


Figure 6. Temperature gradient induced deformation.

4.2 Typical simulation example

Figure 7 shows examples of the stress distributions after cooling for two typical examples: one is the whole solid substrate, and the other is half-solid half-powder, i.e., overhang case. The surrounding powder is not shown since the major focused area is the beam scanning area. The process parameters of the two examples are identical: 1000 mm/sec beam speed, 10 mA beam current and 0.8 mm beam diameter. Figure 7a and Figure 7b show stress contours along the scanning direction for the solid substrate and the overhang case, respectively. For the overhang case, the powder substrate is not shown in order to better illustrate the deformation of the deposited layer in Figure 7b. Figure 7c compares the top surface stress profiles, and it can be noted that the solid substrate case shows a higher stress in the location close to the scanning ends. On the other hand, the overhang case has a lower average stress on the powder substrate compared to the stress in the solid substrate. It can also be observed that for the overhang case, after cooling, the stress above the solid substrate area (left half of the part) is similar to the solid substrate case, except in the area close to the solid/powder substrate interface where a higher stress is observed for the overhang case.

Because of the thermal effect from electron beam scanning and heating, a tensile residual stress is present along the moving direction in the top layer due to powder material contraction during cooling and solidification. Meanwhile, a balancing compressive stress is resulted from the tensile stress in the solid substrate. For the overhang case, because of weak bonding between the solidified materials and the powder substrate, it can be expected that a larger bending moment occurred above the powder substrate side. Moreover, due to a smaller solid substrate area, the bending above the solid substrate is reduced in the overhang case when comparing to the solid substrate case. Figure 8 illustrates the curling conditions discussed, where the overhang case has a larger curling on powder substrate side in the build direction (Y) as well as a larger overall deformation, while a smaller deformation is shown on the solid substrate side.

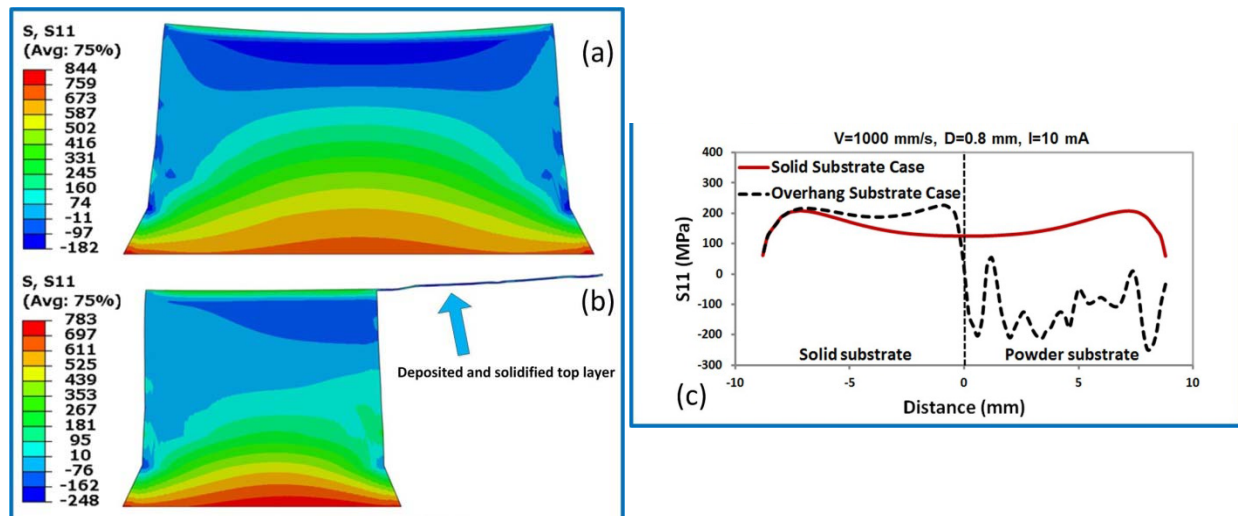


Figure 7. Typical example of residual stress after cooling.

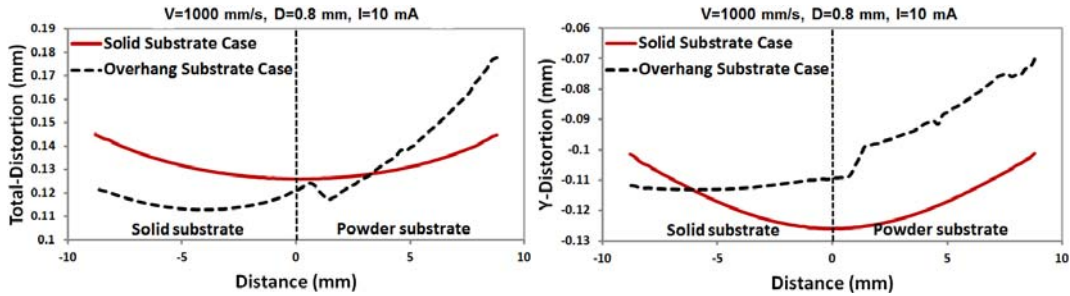


Figure 8. Typical example of deformation profiles (total and Y-direction) after cooling.

4.3 Process parameters effects

With the studied matrix listed in Table 3, some simulation results, stress profile comparisons, are presented in Figure 9. It is noted that different combinations of the beam speed, beam diameter and beam current may noticeably affect the stress and deformation distributions. Specifically, increasing of the beam speed and beam diameter will result in a decrease in Y direction distortions above the powder substrate. Moreover, increasing of the beam current will result in a more severe distortion. It may be concluded that the increase of the energy density, according to Eqn (2), will result in an increase of overhang distortions. On the other hand, increasing of the energy density does not have show a clear trend about the stress distributions above the powder substrate, though slight decrease can be noted above the solid substrate.

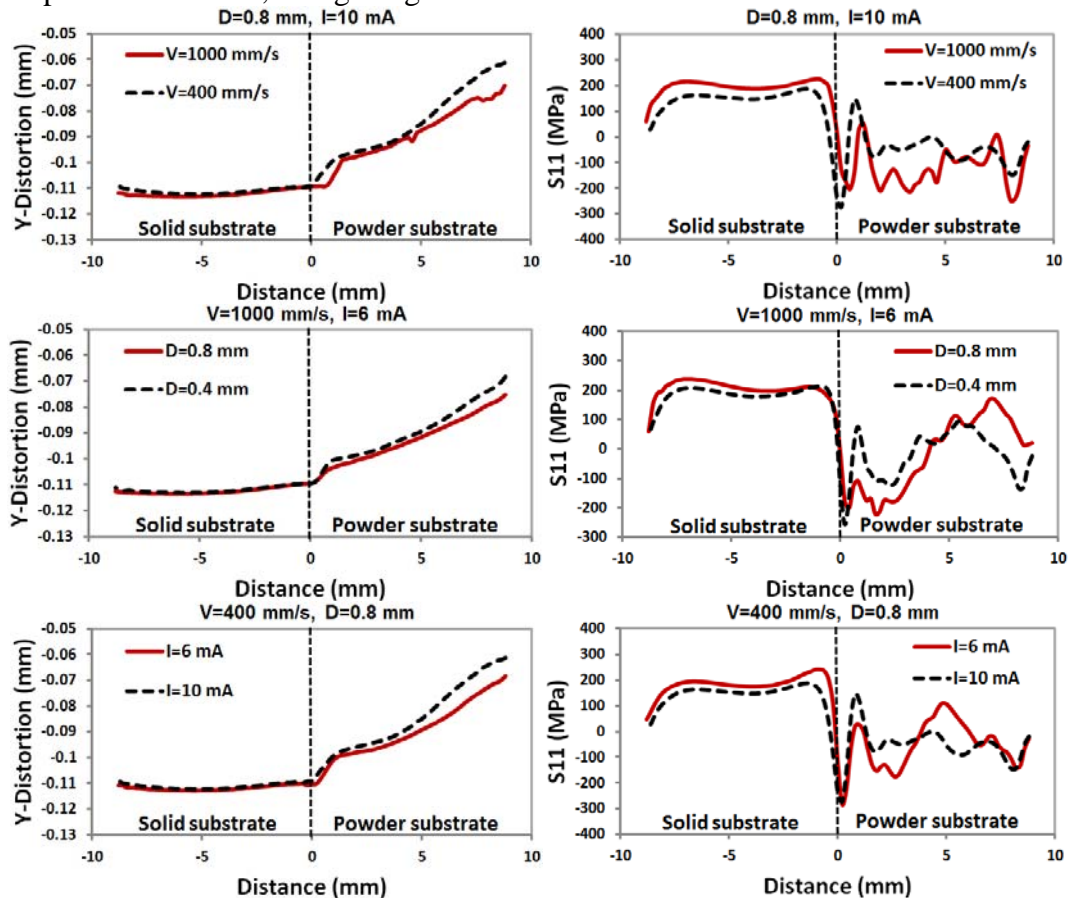


Figure 9. Process parameter effect on overhang distortions and stresses.

The Y-distortion values from all simulation cases were analyzed and plotted against the energy intensity, Eqn (2), of each case. The result is shown in Figure 10 and it is interesting to note an approximately linear relationship between the calculated energy density and the distortion along the build direction. The distortion increases with the increase of the energy density.

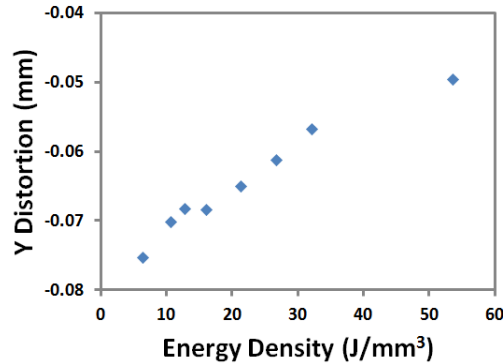


Figure 10. Energy density vs. maximum distortion from different simulation cases.

5. Conclusions

In this study, a 2D FE model of thermomechanical simulations was developed for the EBAM process in building an overhang part. The model incorporated a moving heat source with a Gaussian volumetric intensity, temperature-dependent properties and latent heat of fusion for Ti-6Al-4V, and powder thermal properties, etc. A design of experiments method was implemented to study process parameters effects on thermal stresses and distortions such as curling of an overhang structure. The major findings can be summarized as follows.

(1) In general, the areas above the powder substrate have a lower thermal stress than the areas above the solid substrate.

(2) The resultant distortion in the overhang part above the powder substrate is larger than the distortion above the solid substrate.

(3) With a higher energy density input, e.g., a smaller beam speed, a smaller diameter or a higher beam current, it can result in a more severe curling distortion along the build direction at the overhang area.

Future work will require build part temperature and deformation measurements for comprehensive model validations. In addition, the initial thermal condition for the solid and powder substrates need to be improved in the model, since in the current study, a uniform temperature has been assign for the two sections, it is not clearly that, to what extent, the difference in thermal properties between the solid and powder will cause significantly different preheat temperatures in the two areas.

Acknowledgements

This research is supported by NSF (Award No. 1335481) and NASA (No. NNX11AM11A), and is in collaboration with Marshall Space Flight Center (Huntsville, AL), Advanced Manufacturing Team in Nonmetallic Branch.

References

- [1] Available from: <http://www.arcam.com/>. Accessed June 21, 2013.
- [2] Biamino, S., Penna, A., Ackelid, U., Sabbadini, S., Tassa, O., Fino, P., Pavese, M., Gennaro, P., and Badini, C., 2011, "Electron beam melting of Ti-48Al-2Cr-2Nb alloy: Microstructure and mechanical properties investigation," *Intermetallics*, 19(6), pp. 776-781.
- [3] Gong, X., Anderson, T., and Chou, K., "Review on Powder-Based Electron Beam Additive Manufacturing Technology," ASME/ISCIE 2012 International Symposium on Flexible Automation, St. Louis, MO, June 18-20, 2012, ISFA2012-7256.
- [4] Cormier, D., Harrysson, O., and West, H., "Characterization of H13 steel produced via electron beam melting," Proc. Selected Papers from the 14th Annual Solid Freeform Fabrication Symposium, University of Texas, Austin, Texas, 4-6 August 2003, Emerald Group Publishing Ltd., pp. 35-41.
- [5] Ramirez, D. A., Murr, L. E., Martinez, E., Hernandez, D. H., Martinez, J. L., Machado, B. I., Medina, F., Frigola, P., and Wicker, R. B., 2011, "Novel precipitate-microstructural architecture developed in the fabrication of solid copper components by additive manufacturing using electron beam melting," *Acta Materialia*, 59(10), pp. 4088-4099.
- [6] Murr, L., Martinez, E., Gaytan, S., Ramirez, D., Machado, B., Shindo, P., Martinez, J., Medina, F., Wooten, J., and Ciscel, D., 2011, "Microstructural architecture, microstructures, and mechanical properties for a nickel-base superalloy fabricated by electron beam melting," *Metallurgical and Materials Transactions A*, 42(11), pp. 3491-3508.
- [7] Zäh, M. F., and Lutzmann, S., 2010, "Modelling and simulation of electron beam melting," *Production Engineering. Research and Development*, 4, pp. 15-23.
- [8] Mahale, T. R., 2009, "Electron beam melting of advanced materials and structures," Ph.D. thesis, North Carolina State University, Raleigh, NC.
- [9] Jamshidinia, M., Kong, F., and Kovacevic, R., 2013, "Numerical Modeling of Heat Distribution in the Electron Beam Melting® of Ti-6Al-4V," *Journal of Manufacturing Science and Engineering*, 135(6), p. 061010.
- [10] Shen, N., and Chou, Y. K., 2012, "Thermal modeling of electron beam additive manufacturing process - powder sintering effects," Proceedings of ASME 2012 International Manufacturing Science and Engineering Conference (MSEC), Notre Dame, IN, June 4-8, 2012, MSEC2012-7253.
- [11] Cheng, B., and Chou, K., 2013, "Melt Pool Geometry Simulations for Powder-Based Electron Beam Additive Manufacturing," 24rd Annual International Solid Freeform Fabrication Symposium - An Additive Manufacturing Conference, Austin, TX, USA, August 12-14, 2013.
- [12] Liu, H., Sparks, T. E., Liou, F. W., and Dietrich, D. M., 2013, "Numerical Analysis of Thermal Stress and Deformation in Multi-Layer Laser Metal Deposition Processes," 24rd Annual International Solid Freeform Fabrication Symposium - An Additive Manufacturing Conference, Austin, TX, USA, August 12-14, 2013.
- [13] Kamara, A., Marimuthu, S., and Li, L., 2011, "A numerical investigation into residual stress characteristics in laser deposited multiple layer waspaloy parts," *Journal of Manufacturing Science and Engineering*, 133(3), p. 031013.
- [14] Ding, J., Colegrove, P., Mehnen, J., Ganguly, S., Sequeira Almeida, P., Wang, F., and Williams, S., 2011, "Thermo-mechanical analysis of Wire and Arc Additive Layer

Manufacturing process on large multi-layer parts," *Computational Materials Science*, 50(12), pp. 3315-3322.

[15] Zaeh, M. F., and Branner, G., 2010, "Investigations on residual stresses and deformations in selective laser melting," *Production Engineering*, 4(1), pp. 35-45.

[16] Dai, K., and Shaw, L., 2002, "Distortion minimization of laser-processed components through control of laser scanning patterns," *Rapid Prototyping Journal*, 8(5), pp. 270-276.

[17] Nickel, A., Barnett, D., and Prinz, F., 2001, "Thermal stresses and deposition patterns in layered manufacturing," *Materials Science and Engineering: A*, 317(1), pp. 59-64.

[18] Matsumoto, M., Shiomi, M., Osakada, K., and Abe, F., 2002, "Finite element analysis of single layer forming on metallic powder bed in rapid prototyping by selective laser processing," *International Journal of Machine Tools and Manufacture*, 42(1), pp. 61-67.

[19] Shen, N., and Chou, Y. K., 2012, "Simulations of Thermo-mechanical Characteristics in Electron Beam Additive Manufacturing," *ASME 2012 International Mechanical Engineering Congress & Exposition*, Houston, TX, USA.

[20] Cheng, B., Ping, L., and Chou, K., 2014, "Thermomechanical Investigation of Overhang Fabrications In Electron Beam Additive Manufacturing," *Proceedings of ASME 2014 International Manufacturing Science and Engineering Conference (MSEC)*, Detroit, MI, June 9-13, 2014, MSEC2014-4063.

[21] Boyer, R., Welsch, G., and Collings, E. W., 1998, "Materials Properties Handbook: Titanium Alloys," *ASM International Materials Park, OH, USA*, pp. 483-636.

[22] Rouquette, S., Guo, J., and Le Masson, P., 2007, "Estimation of the parameters of a Gaussian heat source by the Levenberg-Marquardt method: Application to the electron beam welding," *International Journal of Thermal Sciences*, 46(2), pp. 128-138.

[23] Gaytan, S. M., Murr, L. E., Medina, F., Martinez, E., Lopez, M. I., and Wicker, R. B., 2009, "Advanced metal powder based manufacturing of complex components by electron beam melting," *Materials Technology*, 24, pp. 180-190.

[24] Deshpande, A., Tanner, D., Sun, W., Hyde, T., and McCartney, G., 2011, "Combined butt joint welding and post weld heat treatment simulation using SYSWELD and ABAQUS," *Proceedings of the Institution of Mechanical Engineers, Part L: Journal of Materials Design and Applications*, 225(1), pp. 1-10.

[25] Zaeh, M. F., and Kahnert, M., 2009, "The effect of scanning strategies on electron beam sintering," *Production Engineering*, 3(3), pp. 217-224.

[26] Gong, H., Rafi, K., Starr, T., and Stucker, B., 2013, "The Effects of Processing Parameters on Defect Regularity in Ti-6Al-4V Parts Fabricated By Selective Laser Melting and Electron Beam Melting," *24rd Annual International Solid Freeform Fabrication Symposium - An Additive Manufacturing Conference*, Austin, TX, USA, August 12-14, 2013.

[27] Mercelis, P., and Kruth, J.-P., 2006, "Residual stresses in selective laser sintering and selective laser melting," *Rapid Prototyping Journal*, 12(5), pp. 254-265.